Available online at www.sciencedirect.com

ScienceDirect

Ceramics International 39 (2013) 9575–9582

CERAMICS INTERNATIONAL

www.elsevier.com/locate/ceramint

Effect of alumina on the properties of ceria and scandia co-doped zirconia for electrolyte-supported SOFC

Cun Xin Guo, Jian Xin Wang, Chang Rong He, Wei Guo Wang*

Division of Fuel Cell and Energy Technology, Ningbo Institute of Material Technology and Engineering, Chinese Academy of Sciences, 519 Zhuangshi Road, Ningbo 315201, China

Received 25 January 2013; received in revised form 18 March 2013; accepted 18 May 2013
Available online 25 May 2013

Abstract

The properties of ceria and scandia co-doped zirconia electrolytes with different alumina additions were investigated. Microstructure analysis revealed that alumina was an effective sintering aid for ceria and scandia co-doped zirconia. Small addition (< 0.5 wt%) of alumina slightly increased the bulk conductivity. The grain boundary resistance was reduced significantly by alumina addition. Scavenging effect was observed at the grain boundary by element analysis resulting in about 20% increase in the specific grain boundary conductivity. Notable improvement in the flexural strength was measured after the addition of alumina. The sample with 0.5 wt% alumina, exhibiting enhanced grain boundary conductivity and flexural strength, was potential for the application in electrolyte-supported SOFC.

Keywords: C. Ionic conductivity; C. Mechanical properties; D. Al_2O_3; E. Fuel cells

1. Introduction

In recent years, solid oxide fuel cell (SOFC) have been drawing great attentions as a clean energy source with high efficiency on energy transferring [1–3]. Yttria stabilized zirconia is the most common electrolyte used in SOFC [4]. Scandia stabilized zirconia (SSZ) is considered as an alternative to YSZ for its superior high ionic conductivity and stability under both reducing and oxidizing atmosphere at intermediate temperature [5]. Several reports on the ionic conductivity and phase analysis of the scandia–zirconia system indicate that it is a complex system with a phase transition at the temperature around 600 °C [6–8]. From the application point of view, the transformation is not favorable because of the thermal expansion mismatch problems, even if these materials show high oxide ion conductivity. In order to prohibit the phase transition and retain the cubic fluorite structure in scandia doped zirconia, a great deal of research has been conducted on co-doping Sc_2O_3–ZrO_2 with CeO_2, Bi_2O_3, Yb_2O_3, Mn_2O_3, and Ga_2O_3 or Al_2O_3 [9–14]. It has been reported that only one particular composition, 10 mol% scandia and 1 mol% CeO_2 co-doped zirconia (SCSZ), exhibits only cubic phase at both room temperature and SOFC operation temperature [9]. It makes this material an extremely promising option for intermediate temperature (IT) SOFC electrolytes.

For electrolyte-supported SOFC, the mechanical properties and the conductivity of the electrolyte are particularly more important in comparison with that of anode supported SOFC. The use of thinner electrolyte would make the operation temperature lower. Although the mechanical properties of SCSZ is slightly higher than that of YSZ if proceeded properly, at present it seems that the minimum thickness of SCSZ electrolyte that can reliably support a single cell is around 200 μm [15]. In order to lower the thickness, electrolytes with high mechanical properties are required for electrolyte-supported SOFC. Layered electrolytes like YSZ/SCSZ/YSZ and 6SSZ/SCSZ/6SSZ have been designed to improve the mechanical properties [15,16]. The mechanical properties of electrolytes prepared by this approach is evidently enhanced, but the chemical and phase stability is still doubtful at the operation condition. It is well known that the segregation of vitreous phases at the grain boundaries is one of the most important factors in controlling the mechanical properties [17]. Sintering aid usually has positive impact on the mechanical properties of zirconia ceramics. A great number of studies have demonstrated that

*Corresponding author. Tel.: +86 574 87911363; fax: +86 574 87910728.
E-mail address: wgwang@nimte.ac.cn (W.G. Wang).

0272-8842/$ - see front matter © 2013 Elsevier Ltd and Techna Group S.r.l. All rights reserved.
http://dx.doi.org/10.1016/j.ceramint.2013.05.076

alumina is effective in improving the mechanical properties of zirconia electrolytes by changing the chemical composition of the grain boundary [18–20].

As the electrolyte is the principal structural component in electrolyte-supported cells, it is necessary to optimize the conflicting requirements of mechanical strength and ionic conductivity. The grain boundary conductivity of the electrolyte is dramatically affected by the segregation of secondary phases on the grain boundaries [21]. Earlier studies have shown that the silicon-rich amorphous phase is the most common cause for the grain-boundary resistance [21–23]. As SiO_2 is a ubiquitous background impurity in ceramic processing, it is difficult to exclude extrinsic origin even in sample prepared with high grade powders. Although high grade electrolyte powders with very low impurity contents are preferred for SOFC material development, the use of such expensive high grade raw materials results in a serious drawback to cost competitiveness and thus the commercial development of SOFC technology. It has been found that the grain boundary resistance of YSZ can be reduced significantly by the addition of additives such as La_2O_3, Bi_2O_3, and Al_2O_3 [24–26]. The scavenging effect was regarded as the principal contributor to this reduction. However, limited studies were conducted to define this effect on scandia stabilized zirconia.

In this work, the effect of alumina on the microstructure, conductivity and mechanical properties of SCSZ was evaluated for electrolyte-supported SOFC application.

2. Experimental

2.1. Materials and samples

Commercial SCSZ powders (containing ~400 ppm SiO_2, 99.9%, TERIO, China) and fine alumina powders (99.9%, SCRC, China) were used as raw materials to prepare the electrolytes. Different composites of SCSZ/Al_2O_3 with compositions of 0, 0.25, 1, 2 and 5 wt% of alumina were prepared by the conventional tape-casting method followed by lamination and sintering at 1550 °C for 6 h. The samples, in the order of increasing alumina content, were denoted as A00, A02, A05, A10, A20, and A50, respectively.

2.2. Microstructural and phase analysis

Microstructural and elements analysis were performed for each sample using a Hitachi S4800 field emission scanning electron microscope (FE-SEM) equipped with an energy dispersive spectrometer (EDS). An electron probe at an acceleration voltage of 10 kV was employed. A 5 nm Pt film were coated by sputtering before the observation. The X-ray diffraction (XRD) data for the sintered samples were measured by using a Bruker D8 Advance with CuKα radiation at 0.02° s^{-1} steps in the 2θ range of 20–70°.

2.3. Electrochemical tests

The AC impedance spectra of the sintered pellets were measured in the temperature range of 350–800 °C. Platinum paste was brush-painted on both sides of the pellets as electrodes followed by sintering at 850 °C for 3 h. The measurements were taken at 50 °C intervals in air using a Solartron frequency response analyzer (SI 1260) in the frequency range of 0.1–10 MHz at an amplitude of 50 mV. Impedance data evaluation and simulation were performed with the Zview 3.0 software (Scriberner Associates Inc., USA).

2.4. Flexural strength tests

10 Samples for each composition were fractured in three-point bending with a span of 20 mm, at a constant crosshead velocity of 0.3 mm/min using a screw-driven universal testing machine (Instron 4483, Instron, USA). The flexural strength values were extracted from the maximum load, according to the standard recommendations (ASTM-C1161, 1994).

3. Results and discussion

3.1. Microstructure and phase analysis

Fig. 1 shows the top SEM images of samples sintered at 1550 °C in air for 6 h. The average grain sizes of samples, determined by the intercept method, are 6.6, 11.0, 11.6, 11.3, 9.4, and 6.4 μm with adding 0, 0.25, 0.5, 1, 2, and 5 wt% alumina, respectively. It is obvious that the sintering process is promoted by adding a small amount (< 2 wt%) of alumina. As Al^{3+} and Zr^{4+} differ greatly in ionic radius, the solubility limit of alumina in zirconia electrolytes is extremely low [18]. Dopants with different valences and sizes than the host cations as solid solute in stabilized zirconia always act as a growth inhibitor in the sintering process. Tekeli reported that the grain growth in 1 wt% Al_2O_3-doped YSZ ocurred slowly and more sluggish than that of undoped YSZ [27]. Considering that trace impurities of SiO_2, Na_2O and Fe_2O_3 were included in our raw powders, which were prone to form liquid-phases with alumina. The growth of grain size in samples with small alumina concentrations was thus suggested to relate with liquid-phase formations. For high alumina concentrations, corundum alumina phase could be found, which was confirmed by the XRD patterns (Fig. 2). When the content of alumina greatly exceeded the solubility limit, the alumina phase preferentially located at the surfaces of the grains, which was further amplified by segregation during the initial and intermediate stage of sintering. Because the mobility in the alumina-dominated interfaces is low, high alumina concentrations will lead to the decrease in the grain size. As shown in Fig. 2, samples with alumina up to 1 wt% revealed only cubic fluorite reflections, whereas A20 and A50 revealed both cubic fluorite phase and a small quantity of corundum alumina phase. This indicated that cubic structure could be stabilized to room temperature for all samples. No remarkable change of lattice parameters was observed.

3.2. Electrochemical analysis

Impedance spectra of composite electrolytes with Pt electrode were measured in air in the temperature range of 350–800 °C. The results measured at 350 °C are shown in Fig. 3. According to the

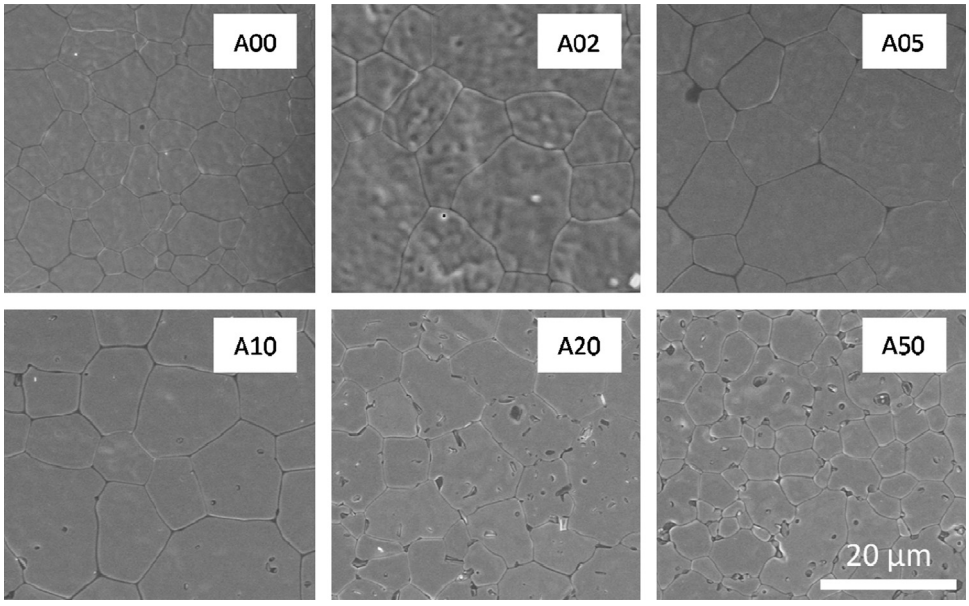

Fig. 1. SEM micrograph of samples sintered at 1550 °C for 6 h.

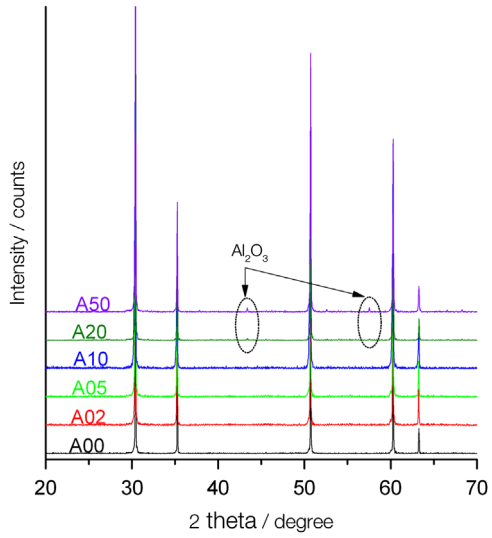

Fig. 2. XRD patterns of samples containing different alumina contents.

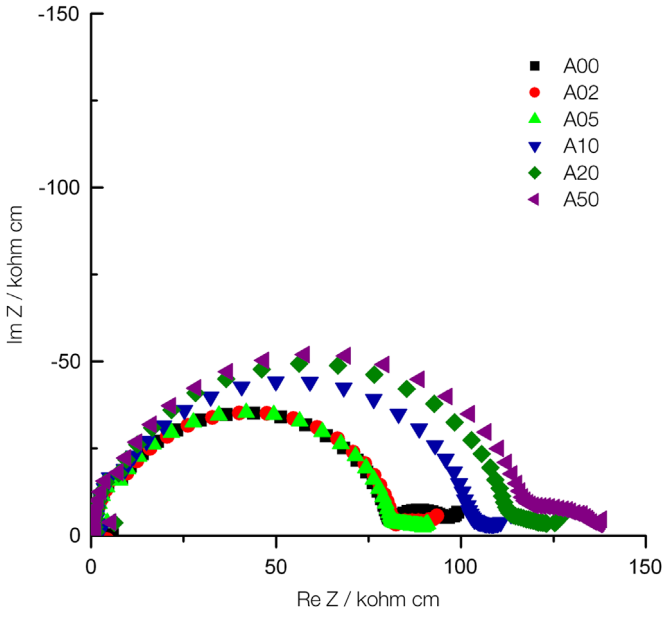

Fig. 3. Impedance spectra of samples measured at 350 °C.

brick layer model, semicircles that belonged to the grain interior and the grain boundary were clearly observed at different frequency ranges. Impedance spectra showed that small addition (up to 0.5 wt%) of alumina had little influence on the bulk (grain interior) resistance. The bulk resistances (R_{bulk}) of A00, A02 and A05 were 80.4, 80.6, 81.0 kΩ cm, respectively, increasing slightly with increasing alumina content. Higher alumina content, however, caused a pronounced increase in bulk resistance. Considering that the fraction of alumina phase is low, even for samples with higher alumina concentrations, the bulk effects on the bulk conductivity should be insignificant. This significant decrease in bulk conductivity could be mainly traceable to current detour around alumina phase [28]. Beyond this, the addition of alumina also made a great impact on the grain boundary resistance (R_{gb}). The grain boundary resistance of the reference sample without alumina addition was 17.6 kΩ cm. As shown in Fig. 3, a significant reduce in grain boundary resistance could be observed. A10 and A20 had the least resistance around 5.8 kΩ cm, approximately one-third of that of A00. Thus, the electrochemical properties of the electrolytes were significantly improved by small alumina addition at low temperature. For higher alumina concentrations, the low frequency "semicircles" became distinctly distorted and its size increased with increasing alumina content. This implied that current constriction became important and a simple brick layer analysis fails in such case [29].

Fig. 4 shows the temperature dependence of the total ionic conductivity for all samples. The total conductivity was calculated by $\sigma_{tol}=L/(AR)$, where L is the thickness of the pellet, A is the surface area of the pellet and R is the total resistance which is determined by the summation of grain boundary resistance and bulk resistance. It was noticed that the plot could not be fitted by a single straight line. The curve exhibited different slopes in the low- and high-temperature range at a transitional point at around 550 °C. This implied that the mechanism of ionic conduction was changed at this temperature. The change of the activation energy at different temperatures range could be explained by the change in conduction mechanism in the high- and low-temperature range [12]. With the increasing of temperature, the conductivity increased without any abrupt change. At temperatures below 500 °C, the samples containing alumina up to 0.5 wt% exhibited higher conductivity than that of A00 caused by the considerable reduce in the grain boundary resistance. At the elevated temperature, although the increase in the bulk resistance by alumina addition resulted in a decrease in the total conductivity, the difference of that between A00, A02 and A05 was very small. This indicated that small addition of alumina was acceptable on the consideration of conductivity.

Fig. 5 shows the composition dependence of the activation energy for oxygen ionic conduction at low- and high-temperature range. The activation energy at low-temperature range was always higher than that at high-temperature range. The effect of Al^{3+} dopant on the activation energy at different temperature range was entirely different. In the temperature range 350–500 °C, the activation energy decreased with the addition of alumina. A10 exhibited the lowest activation energy of 1.483 eV at this temperature range. In the temperature range of 600–800 °C, on the contrary, the activation energy increased linearly with the increase of alumina up to 1 wt%. Samples with higher alumina content showed almost the same activation energy as A10. At low temperature, the diffusion of oxygen vacancies is affected by the elastic strain energy, which is related to the size mismatch between the host and dopant cation. Associate defects can easily occur at low temperature suppressing the migration of oxygen vacancies. At high temperature the defects are completely dissociated and the isolated oxygen vacancies can migrate freely.

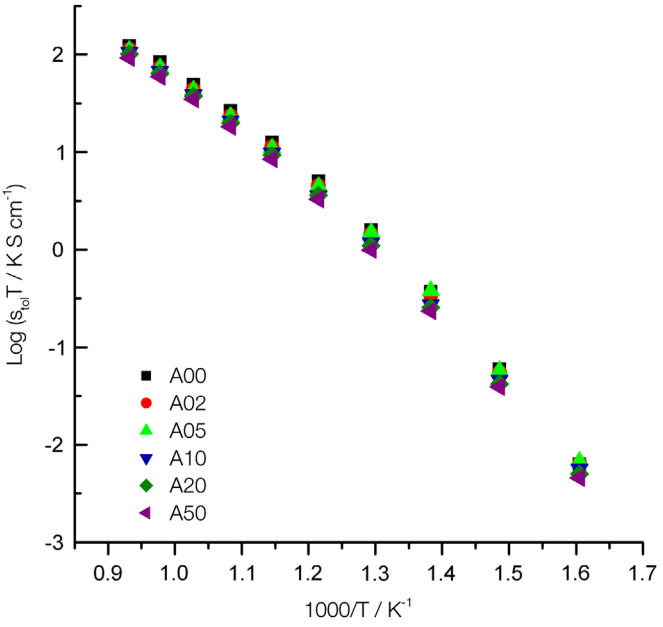

Fig. 4. The total ionic conductivity as a function of the temperature and alumina content.

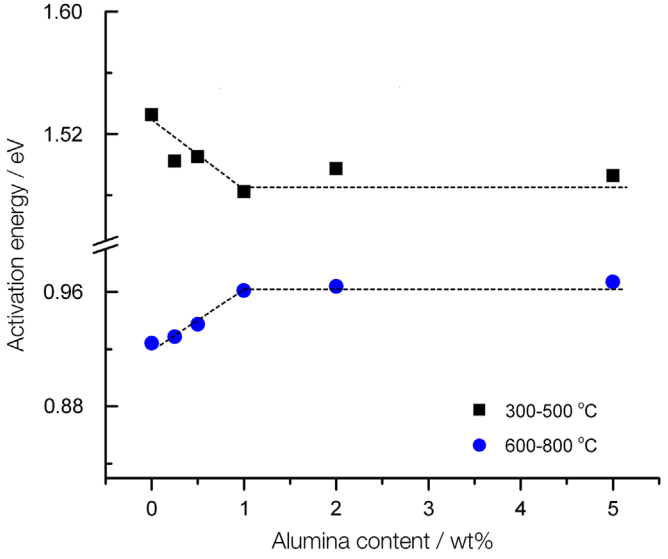

Fig. 5. The calculated activation energy for ionic conduction as a function of alumina content.

As a grain boundary resistance was hard to separate from a bulk resistance in an impedance spectra at high temperatures, the bulk (σ_{bulk}) and the apparent grain boundary ($\sigma_{gb}^{app}=L/R_{gb}A$) conductivities of samples as determined by application of impedance spectroscopy were also depicted as a function of temperature in the range of 350–500 °C. In Fig. 6, alumina conduced to a decrease in the bulk conductivity of SCSZ. The same effect has been discovered on YSZ electrolytes [23]. More obvious decrease could be observed at higher temperatures. As shown in Fig. 7, evident enforcement in the apparent grain boundary conductivity could be seen except for A50. Unlike the bulk conductivity, the effect of alumina on the apparent grain boundary conductivity was very similar at any temperature.

Because σ_{gb}^{app} depended on the grain sizes, σ_{gb}^{sp} was estimated to remove the effects of grain sizes. According to the block-layer model, σ_{gb}^{sp} caculated from the average grain size d_g and average grain boundary thickness δ_{gb}, was given by the equation [26]

$$\sigma_{gb}^{sp}=\sigma_{gb}^{sp}\frac{\delta_{gb}}{d_g} \quad (1)$$

Since δ_{gb} was difficult to determinate and lay almost constant within a fairly narrow range of 1–2 nm, σ_{gb}^{sp} was generally alternatively represented by σ_{gb}^{app}/d_g. Fig. 8 illustrates the specific grain boundary conductivity as a function of the

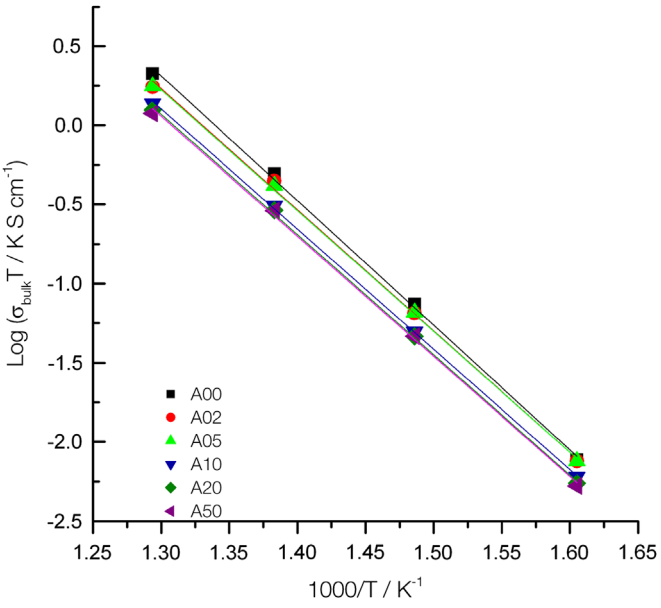

Fig. 6. The bulk conductivity as a function of the temperature and alumina content.

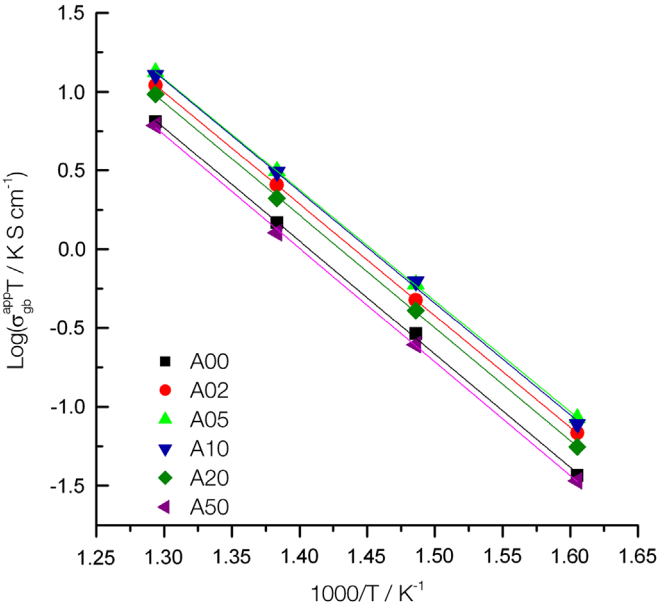

Fig. 7. The apparent grain boundary conductivity as a function of the temperature and alumina content.

temperature. A slight gain on the specific grain boundary conductivity was observed with alumina up to 1 wt%. A05 and A10 showed the maximum conductivity over the entire temperature range measured. Guo et al. [23] reported that the addition of 0.4 mol% Al_2O_3 in high pure YSZ decreased the grain boundary conductivity by 600%. However, a reverse result has been reported by Lee et al. [26]. The forming of inclusions containing Si was considered to be the origin of scavenging. Considering the existence of 400 ppm SiO_2 in SCSZ powders, dramatic enhancement on σ_{gb}^{sp} of SCSZ resulting from scavenging effect by alumina addition was expected. However, the maximum specific grain boundary

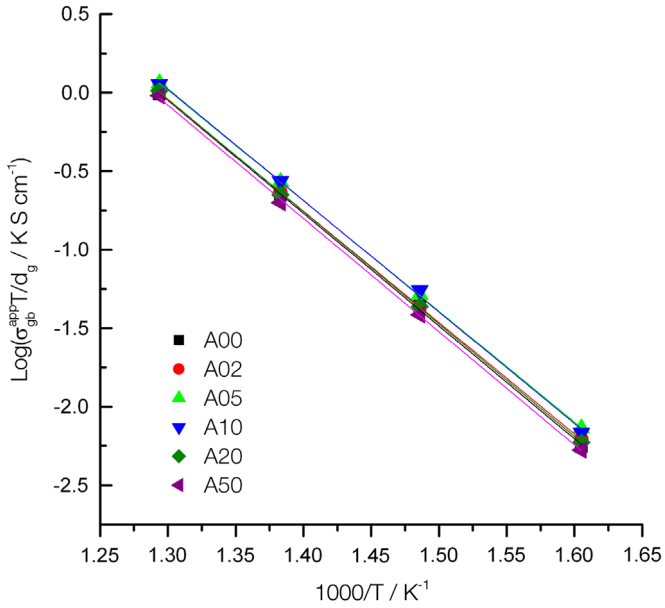

Fig. 8. The specific grain boundary conductivity as a function of the temperature and alumina content.

conductivity in alumina doped SCSZ was only about 20% higher than that of the undoped one.

To get further insight into the effect of alumina on the grain boundary conductivity, the composition of the grain boundary of A10 was studied by scanning electron microscopy combined with energy dispersive X-ray spectroscopy (EDS) (Fig.9). As shown in Fig. 9a, a small quantity of alumina phase (dark area) was detected at the grain boundaries. EDS analysis showed that yielding precipitates rich in Al, and Si, and with indication of depleted Zr was formed at multiple grain–grain contacts or grain boundaries. Sodium, a common element in raw zirconia materials, was also detected. The mechanism of this scavenging effect is still under research [30,31], but we may speculate that the extra alumina has a tendency to react with secondary phases segregated at the grain boundaries. The results revealed that the scavenging effect of alumina could not make a considerable increase in grain boundary conductivity of SCSZ. The significant decrease in grain boundary resistance was ascribed to both size and scavenging effect. Since the alumina phase was preferentially located at the grain boundaries, the significant current constrictions may be ascribed to the variation of the specific grain boundary conductivity for higher alumina contents [28,29].

Fig. 10 shows the calculated activation energy for bulk and grain boundary conduction as a function of alumina content at the temperature range 350–500 °C. Because the substitution of Al^{3+} was much lower than that of Sc^{3+}, the E_{bulk} value was mainly determined by Sc^{3+}. The activation energy for bulk conduction was in the range of 1.50–1.57 eV, which was much higher than that of YSZ [32]. The activation energy of bulk conductivity decreased slightly after the addition of alumina. At this temperature range, oxygen vacancies were associated with dopant ions (Sc^{3+}, Ce^{4+}, Al^{3+}), and the activation energy consisting of the association enthalpy and the migration

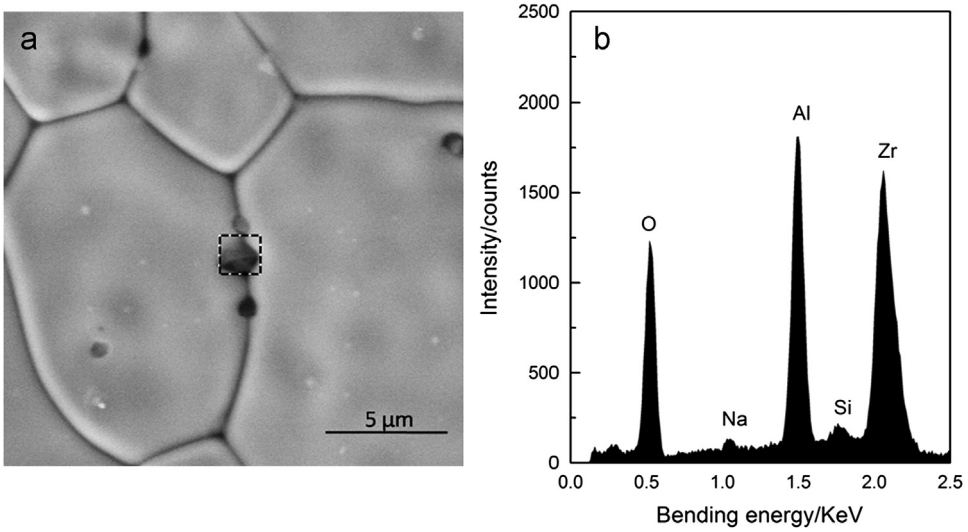

Fig. 9. SEM image and EDS pattern of the grain boundary of sample with 1 wt% alumina.

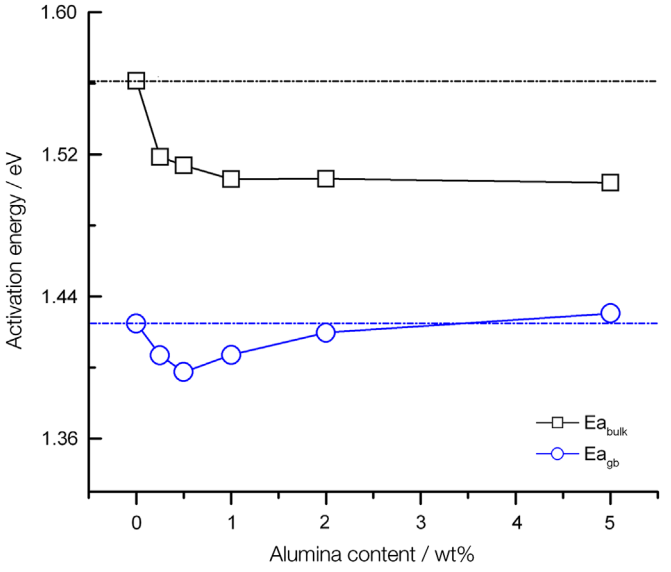

Fig. 10. The calculated activation energy for bulk and grain boundary conduction at the temperature range 350–500 °C as a function of alumina content.

enthalpy of oxide ion. The substitution of dopant Al^{3+} ion induced the increase of the association enthalpy, because the difference between the ionic radius of Al^{3+}(0.53 Å) and Zr^{4+} (0.84 Å) is much larger compared to that of Sc^{3+}(0.84 Å) and Zr^{4+}. Thus, the increase of the association enthalpy might be the key factor in the decrease of the activation energy for bulk conduction. The activation energy for grain boundary conduction also somewhat decreased when alumina was added. A05 showed the lowest activation energy of 1.398 eV. In a space charge layer model, the oxygen vacancy depletion in the space charge layer is proposed as the cause of the "intrinsic" grain boundary blocking effect [22,23]. The ionic conduction is expected to occur through the grain–grain contacts. Additional phases are suggested not to alter the grain boundary conduction mechanism, rather to reduce the contacts by blocking the boundary area. For alumina up to 1 wt%, the grain boundary was homogeneous without alumina secondary phase. The depletion was changed by the alumina addition, which resulted in the decrease of the activation energy of grain boundary conductivity. For higher alumina contents, current detour effects around the insulating alumina phase play a great role and contribute to the grain boundary resistance (current constriction). Note that insulating alumina phase located at grain boundaries and Ea_{gb} is close to Ea_{bulk} for higher alumina concentrations. Consequently the so-calculated activation energy no longer reflects the real activation energy of grain boundary conductivity.

3.3. Flexural strength test

Fig. 11 shows the average flexural strength measured by a three-point test as a function of the alumina content. The specimen thickness, the homogeneity and porosity of the material, and the loading rate are important parameters affecting the results. Thus, we have to point out that the sample thicknesses were nearly 200 μm prepared by the tape-casting method. This was a nonstandard thickness for flexural strength test, but it could reflect the practical situation of the electrolytes used in the self-supported SOFC. The electrolyte without any addition of alumina showed a flexural strength of 390 MPa, in conformity with that reported elsewhere [33]. The flexural strength was greatly improved when alumina was introduced. A significant increase in flexural strength from 390 MPa to 500 MPa was occured when 0.5 wt% alumina was added, and it came to the highest flexural strength of 536 MPa for A50. Because micro-cracks always extended along the grain boundaries, the variation of the grain boundary phases would substantially influence the flexural strength. Enhancing the grain–grain contact by promoting sintering and scavenging siliceous phase by addition of alumina were put forward to account for this. Furthermore, the high elastic modulus of

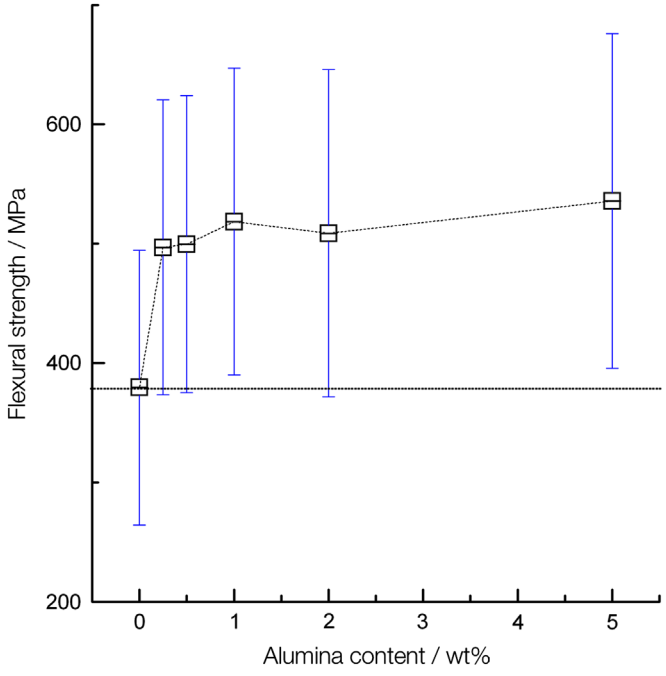

Fig. 11. The flexural strength as a function of alumina content.

alumina was regarded as another important factor affecting flexural strength [26].

4. Conclusions

Effect of alumina on the microstructure, conductivity and flexural strength of ceria and scandia co-doped zirconia was investigated. Alumina was an effective sintering aid for SCSZ. Small addition of alumina (< 1 wt%) considerably reduced the grain boundary resistance and slightly increased the bulk resistance. Scavenging effect was confirmed by EDS analysis, but only about 20% enhancement in the specific grain boundary conductivity was observed. This significant decrease in grain boundary resistance might be due to both the grain growth and the enhanced grain–grain contact caused by scavenging siliceous phases. For higher alumina concentrations, alumina had negative effects both on buck and grain boundary conductivity. Significant current constrictions around insulating alumina phase should account for this. Significant enhancement of flexural strength was observed for all samples with alumina addition. The sample containing 0.5 wt% alumina, exhibiting good conductivity and enhanced flexural strength, shows great potential for electrolyte-supported SOFC application.

Acknowledgments

An earlier version of this paper was presented at 10th European SOFC Forum. This study was accomplished in the Ningbo Institute of Material Technology & Engineering, Chinese Academy of Sciences, and was financially supported by the National Natural Science Foundation of China (No. 50902135) and the Natural Science Foundation of Ningbo (No. 2010A610148). This work was also partly supported by the China Postdoctoral Science Foundation (2012M521208), Zhejiang Provincial Advanced Postdoctoral Scientific Program (Bsh1201010). Colleagues at the Division of Fuel Cell & Energy Technology were acknowledged for their assistance in the manufacturing of the electrolyte.

References

[1] M. Williams, Solid oxide fuel cells: fundamentals to systems, Fuel Cells 7 (1) (2007) 78–85.
[2] E. Ivers-Tiffée, A. Weber, D. Herbstritt, Materials and technologies for SOFC-components, Journal of the European Ceramic Society 21 (10) (2001) 1805–1811.
[3] H. Yokokawa, et al., Recent developments in solid oxide fuel cell materials, Fuel Cells 1 (2) (2001) 117–131.
[4] Y. Mizutani, et al., Development of high-performance electrolyte in SOFC, Solid State Ionics 72 (1994) 271–275.
[5] S. Badwal, F. Ciacchi, D. Milosevic, Scandia–zirconia electrolytes for intermediate temperature solid oxide fuel cell operation, Solid State Ionics 136 (2000) 91–99.
[6] K. Nomura, et al., Aging and Raman scattering study of scandia and yttria doped zirconia, Solid State Ionics 132 (3–4) (2000) 235–239.
[7] C. Haering, et al., Degradation of the electrical conductivity in stabilised zirconia system: Part II: scandia-stabilised zirconia, Solid State Ionics 176 (3–4) (2005) 261–268.
[8] O. Yamamoto, et al., Electrical conductivity of stabilized zirconia with ytterbia and scandia, Solid State Ionics 79 (1995) 137–142.
[9] S. Omar, et al., Ionic conductivity ageing investigation of 1Ce10ScSZ in different partial pressures of oxygen, Solid State Ionics 184 (1) (2010) 2–5.
[10] M. Hirano, et al., Effect of Bi_2O_3 additives in Sc stabilized zirconia electrolyte on a stability of crystal phase and electrolyte properties, Solid State Ionics 158 (3) (2003) 215–223.
[11] C. Varanasi, et al., Electrical conductivity enhancement in heterogeneously doped scandia-stabilized zirconia, Journal of Power Sources 147 (1–2) (2005) 128–135.
[12] F. Yuan, et al., Investigation of the crystal structure and ionic conductivity in the ternary system $(Yb_2O_3)_x$–$(Sc_2O_3)_{(0.11-x)}$–$(ZrO_2)_{0.89}$ ($x=0$–0.11), Journal of Alloys and Compounds (2013) 200–205549 (2013) 200–205.
[13] Z. Lei, Q. Zhu, Phase transformation and low temperature sintering of manganese oxide and scandia co-doped zirconia, Materials Letters 61 (6) (2007) 1311–1314.
[14] Y. Arachi, et al., Electrical conductivity of ZrO_2–Sc_2O_3 doped with HfO_2, CeO_2, and Ga_2O_3, Journal of the Electrochemical Society 148 (5) (2001) A520–A523.
[15] Y. Chen, et al., Layered YSZ/SCSZ/YSZ electrolytes for intermediate temperature SOFC Part I: design and manufacturing, Fuel Cells 12 (5) (2012) 722–724.
[16] Seabaugh, M.M., et al., Supported ceramic membranes and electrochemical cells and cell stacks including the same, US Patents 7,767,358, 2010.
[17] K. Das, G. Banerjee, Mechanical properties and microstructures of reaction sintered mullite–zirconia composites in the presence of an additive-dysprosia, Journal of the European Ceramic Society 20 (2) (2000) 153–157.
[18] X. Guo, Roles of alumina in zirconia for functional applications, Journal of the American Ceramic Society 86 (11) (2003) 1867–1873.
[19] A. Larrea, et al., Microstructure and mechanical properties of Al_2O_3–YSZ and Al_2O_3–YAG directionally solidified eutectic plates, Journal of the European Ceramic Society 25 (8) (2005) 1419–1429.
[20] S. Choi, N. Bansal, Mechanical behavior of zirconia/alumina composites, Ceramics International 31 (1) (2005) 39–46.

[21] M. Aoki, et al., Solute segregation and grain-boundary impedance in high-purity stabilized zirconia, Journal of the American ceramic society 79 (5) (2005) 1169–1180.
[22] X. Guo, J. Maier, Grain boundary blocking effect in zirconia: a Schottky barrier analysis, Journal of the Electrochemical Society 148 (2001) E121.
[23] X. Guo, et al., Role of space charge in the grain boundary blocking effect in doped zirconia, Solid State Ionics 154 (2002) 555–561.
[24] T. Carvalho, et al., Lanthanum oxide as a scavenging agent for zirconia electrolytes, Solid State Ionics 225 (4) (2012) 484–487.
[25] S. Sarat, N. Sammes, A. Smirnova, Bismuth oxide doped scandia-stabilized zirconia electrolyte for the intermediate temperature solid oxide fuel cells, Journal of Power Sources 160 (2) (2006) 892–896.
[26] J.H. Lee, et al., Improvement of grain-boundary conductivity of 8 mol% yttria-stabilized zirconia by precursor scavenging of siliceous phase, Journal of the Electrochemical Society 147 (7) (2000) 2822–2829.
[27] S. Tekeli, Influence of alumina addition on grain growth and room temperature mechanical properties of 8YSCZ/Al_2O_3 composites, Composites Science and Technology 65 (6) (2005) 967–972.
[28] J. Fleig, J. Maier, The impedance of ceramics with highly resistive grain boundaries: validity and limits of the brick layer model, Journal of the European Ceramic Society 19 (6) (1999) 693–696.
[29] J. Fleig, The influence of non-ideal microstructures on the analysis of grain boundary impedances, Solid State Ionics 131 (1) (2000) 117–127.
[30] A. Hassan, et al., Influence of alumina dopant on the properties of yttria-stabilized zirconia for SOFC applications, Journal of Materials Science 37 (16) (2002) 3467–3475.
[31] J.H. Lee, et al., Imaging secondary-ion mass spectroscopy observation of the scavenging of siliceous film from 8-mol%-yttria-stabilized zirconia by the addition of alumina, Journal of the American Ceramic Society 83 (5) (2000) 1273–1275.
[32] B. Kumar, et al., Electrical properties of heterogeneously doped yttria stabilized zirconia, Journal of Power Sources 140 (1) (2005) 12–20.
[33] Hata, K. N. Aikawa, Process for production of scandia-stabilized zirconia sheet, scandia-stabilized zirconia sheet obtained by the process, and scandia-stabilised zirconia sintered powder, EP Patent 2,492,257, 2012.